Journal of Structural Geology 30 (2008) 1383–1395

Contents lists available at ScienceDirect

Journal of Structural Geology

journal homepage: www.elsevier.com/locate/jsg

Heterogeneous shear zone evolution: The role of shear strain hardening/softening

Stefano Vitale*, Stefano Mazzoli

Dipartimento di Scienze della Terra, Università degli studi di Napoli 'Federico II', Largo San Marcellino 10, 80138 Napoli, Italy

ARTICLE INFO

Article history:
Received 23 January 2008
Received in revised form 16 July 2008
Accepted 18 July 2008
Available online 5 August 2008

Keywords:
General shear
Strain localization
Strain rate
Displacement rates

ABSTRACT

Mathematical models are proposed to describe heterogeneous shear zones characterized by variation thickness with time. These models take into account several combinations of deformation type regime (simultaneous simple shear, pure shear, and volume change) and degree of strain localization. Increasing or decreasing shear zone thickness results, respectively, from strain hardening where deformation progressively diffuses into the host rock, and strain softening where deformation gradually localizes within a narrow zone. Shear zone models are made of a series of layers, each characterized by homogenous strain. A quantitative evaluation of displacement–thickness relationship and finite strain development may be obtained from each model. Temporal evolution depends on the following parameters: (i) rate of shear strain hardening/softening, (ii) initial shear strain increment imposed to the system, and (iii) thickness of homogenously deformed units within a layered shear zone. Based on data coming from natural shear zones, displacement rates may be obtained independently of shear zone thickness.

1. Introduction

Shear zones are extensively studied geological structures. They develop in a wide range of P–T conditions and show a large variety of geometries, dimensions and related meso- and microstructures. In their pioneering work, Ramsay and Graham (1970) showed that the only possible localized deformation, characterized by parallel, planar shear boundaries is produced by simple shear and/or volume change, while a localized pure shear creates strain incompatibility between the shear zone and its wall rock. Geometric incompatibility is even more pronounced when the intensity of pure shear component is variable across the shear zone, since the overall displacement must be accommodated along discontinuities between homogeneously deformed layers (*cream cake effect*, Ramsay and Huber, 1987). On the other hand, several studies suggested the synchronous occurrence of simple shear, pure shear and/or volume change (Srivastava et al., 1995; Ring, 1998; Baird and Hudleston, 2007; Horsman and Tikoff, 2007). The resulting strain combination has been modelled by Fossen and Tikoff (1993). However, the latter model describes homogeneous shear zones, while it is largely reported that most natural shear zones show heterogeneous deformation (e.g. Ramsay and Graham, 1970; Ramsay, 1980; Ramsay and Huber, 1987). The heterogeneity deformation is pointed out by the variability of some strain parameters, such as strain ratio (ellipticity) and shear strain, and is generally characterized by the increase of the strain intensity from the margins to the middle part of the shear zone. A common approach used in recent years in the study of heterogeneous shear zones is the subdivision of the deformed rock in homogeneously deformed volumes, and the application of matricial algebra rules (e.g. Horsman and Tikoff, 2007).

Heterogeneous shear zones can be classified into three types based on their thickness change with time (Means, 1984, 1995; Hull, 1988; Horsman and Tikoff, 2007). Type I corresponds to shear zones showing increasing thicknesses; type II includes shear zones displaying decreasing thicknesses and type III is characterized by a constant thickness. All models are based on the assumption that shear zones result from the temporal evolution of an original shear zone that may vary in thickness during deformation. From this point of view, shear zones record the whole deformation history and therefore, choosing suitable models, it is possible to reconstruct realistic strain paths (Horsman and Tikoff, 2007).

A useful tool to discriminate among the previously mentioned shear zone types is the pattern of shear strain gradient (Hull, 1988; Fig. 1). For type I, the finite shear strain configuration is a flat-topped curve; for type II, it has a peaked shape; while for type III the shear strain is constant throughout the shear zone. Type I must be driven by processes allowing the shear zone to thicken with time, i.e. to strain harden (Means, 1995). The original shear zone, being not able to accumulate large strains, thickens and new volumes of

* Corresponding author. Tel.: +39 (0)812538124; fax: +39 0815525611.
E-mail address: stvitale@unina.it (S. Vitale).

0191-8141/$ – see front matter © 2008 Elsevier Ltd. All rights reserved.
doi:10.1016/j.jsg.2008.07.006

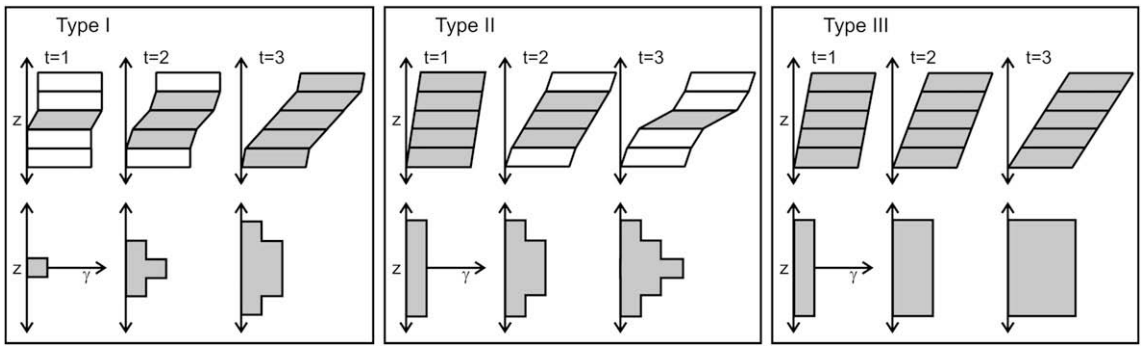

Fig. 1. Representation of the three shear zone types defined by Hull (1988), showing shear strain profiles across the shear zones.

rock located along the margins deform. Conversely, type II involves strain softening, allowing the inner part of the shear zone to accumulate more strain with respect to the margins that become inactive with time. Strain hardening or softening implies that variable shear strain rates or longitudinal strain rates occur with time, meaning that deformation is not steady state. However, most mathematical models of shear zones assume kinematic and geometric parameters that are not time-dependent. The aim of this paper is to provide a simple mathematical model for shear zones showing increasing (type I) or decreasing (type II) thicknesses, taking into account the variability of the incremental deformation due to strain hardening or softening. In order to encompass a wide range of shear zones, several combinations of deformation types and strain localizations are considered. The first part of this study is addressed at obtaining a matricial representation of finite strain for each shear zone model. In the second part, a simple strain function is applied in order to obtain models that can be compared with real data from natural shear zones.

2. From homogeneous to heterogeneous shear zone models

A general homogeneous deformation can be represented by the strain matrix (Fossen and Tikoff, 1993):

$$A = \begin{pmatrix} k_1 & \Gamma_{12} & \Gamma_{13} \\ 0 & k_2 & \Gamma_{23} \\ 0 & 0 & k_3 \end{pmatrix} \quad (1)$$

where k_1, k_2 and k_3 are elongations along the X, Y and Z principal axes of the strain ellipsoid, respectively, and Γ_{12}, Γ_{13} and Γ_{23} are effective shear strain components describing the rotational part of the deformation. In this study, we consider a shear zone characterized by shear planes parallel to the xy plane of the coordinate system, with shear and stretching along the x axis ($\Gamma_{12} = \Gamma_{23} = 0$ and $\Gamma_{13} \neq 0$), and shortening along the z axis ($k_2 = 1$ and $k_1 k_3 = 1 + \Delta$, where Δ is the not positive volume change and $k_1 \geq 1$). This configuration corresponds to a monoclinic shear zone (i.e. a thrust in the x direction) with no deformation along the y axis. It is represented by the strain matrix (Fossen and Tikoff, 1993):

$$A = \begin{pmatrix} k_1 & 0 & \Gamma_{13} \\ 0 & 1 & 0 \\ 0 & 0 & k_3 \end{pmatrix} \text{ where } \Gamma_{13} = \frac{\gamma(k_1 - k_3)}{\ln\left(\frac{k_1}{k_3}\right)} \text{ and } \gamma \text{ is the strain} \quad (2)$$

The deformation may be localized in the shear zone or involve the whole rock. In the latter case, the wall rock may be affected by pure shear and/or volume change.

In order to model a heterogeneous shear zone of type I, we consider a temporal succession of homogeneous deformation stages affecting an increasing number of layers; i.e. for a symmetrical configuration, an original shear zone increasing its thickness with time at the expense of both margins (Fig. 2). On the contrary, to model a type II shear zone we consider the same homogeneous deformation affecting a progressively decreasing number of layers (Fig. 3). Taking into account all possible combinations of deformation types and strain localization modes, both type I and type II shear zones have been divided into three subtypes. Types Ia and IIa are characterized by simple shear alone (Figs. 2a and 3a). Types Ib and IIb involve general shear within the shear zone, as well as pure shear and/or volume change affecting the wall rock (Figs. 2b and 3b). In this case, the presence of a pure shear component does not introduce strain incompatibility between single layers because the elongation along the x direction attains the same value both within the shear zone and in the host rock. In the following, several subgroups will be distinguished: those characterized by general shear involving simple shear and simultaneous pure shear with strain hardening (type Ib1) or strain softening (type IIb1), and those involving simple shear and simultaneous volume change with strain hardening (type Ib2) or strain softening (type IIb2). Types Ic and IIc imply general shear localized within the shear zone (Figs. 2c and 3c). In contrast to previous models, here the presence of a pure shear component introduces strain incompatibility inside the shear zone because different elongations affect different portions of the structure. Also in this instance, subgroups have been considered: those being characterized by simple shear and localized pure shear (types Ic1 and IIc1), and those involving simple shear and localized volume change (types Ic2 and IIc2).

2.1. Types Ia and IIa: localized simple shear

We first consider a homogeneous deformation characterized by time-dependent simple shear ($k_1 = k_2 = k_3 = 1$ and $\gamma > 0$), represented by the incremental strain matrix $A(t)$:

$$A(t) = \begin{pmatrix} 1 & 0 & \gamma(t) \\ 0 & 1 & 0 \\ 0 & 0 & 1 \end{pmatrix} \quad (3)$$

In order to simulate strain hardening (type I shear zones), the strain matrix A must change as a function of time, with decreasing shear strain intensity. For a discrete case, the succession of incremental strain matrices $A(1)\ldots A(t)\ldots A(n)$ must be related by the relationship $\gamma(t+1) < \gamma(t)$. In this instance, the strain path for each layer of the model shear zone is non-steady-state because geometric strain parameters (such as the orientation of the incremental strain ellipse axes) and kinematic parameters (such as shear strain rate or displacement rate) change with time. For n steps, a symmetric shear zone is divided in $(2n-1)$ layers. In the following, asterisk apex indicates a finite quantity.

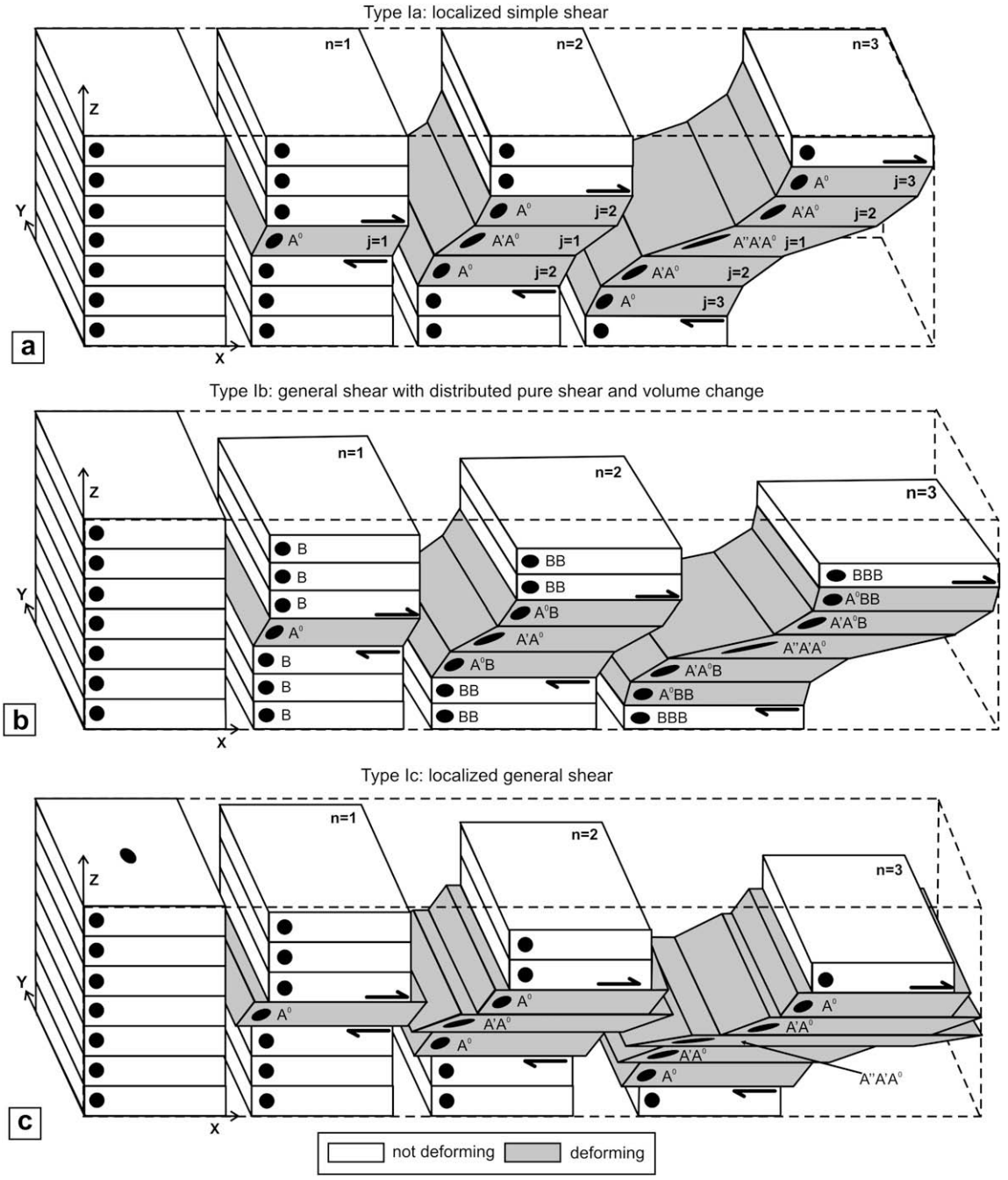

Fig. 2. Schematic evolution of shear zones characterized by increasing thickness with time (shear strain hardening). The succession of finite strain accumulation is labelled in each layer as the product of the incremental strain matrix (see text). (a) Type Ia: localized simple shear. (b) Type Ib: localized general shear with distributed pure shear and volume change. (c) Type Ic: localized general shear.

For layer j (with j ranging between 1 and n), the finite strain matrix $A^*_{\mathrm{Ia}}(j)$ is the product of the first $(n-j+1)$ incremental strain matrices $A(t)$. Therefore, after n steps for type Ia shear zones the finite strain matrix is:

$$A^*_{\mathrm{Ia}}(j) = \prod_{i=0}^{n-j} \begin{pmatrix} 1 & 0 & \gamma(i) \\ 0 & 1 & 0 \\ 0 & 0 & 1 \end{pmatrix} = \prod_{i=0}^{n-j} A(i) \tag{4}$$

This equation can be applied also to type IIa shear zones (although the correspondence between j indexes and layers is different; compare Figs. 2 and 3). Furthermore, for strain softening and localization to occur, the succession of incremental strain matrices $A(1)\ldots A(t)\ldots A(n)$ must be related by the relationship: $\gamma(t+1) > \gamma(t)$. Figs. 2(a) and 3(a) illustrate the temporal evolution of the modelled type Ia and IIa shear zones for $n = 3$.

2.2. Types Ib and IIb: localized general shear, distributed pure shear and volume change

In order to model these shear zone types, we consider an incremental matrix A describing localized general shear:

$$A(t) = \begin{pmatrix} k_1 & 0 & \Gamma(t) \\ 0 & 1 & 0 \\ 0 & 0 & k_3 \end{pmatrix} \tag{5}$$

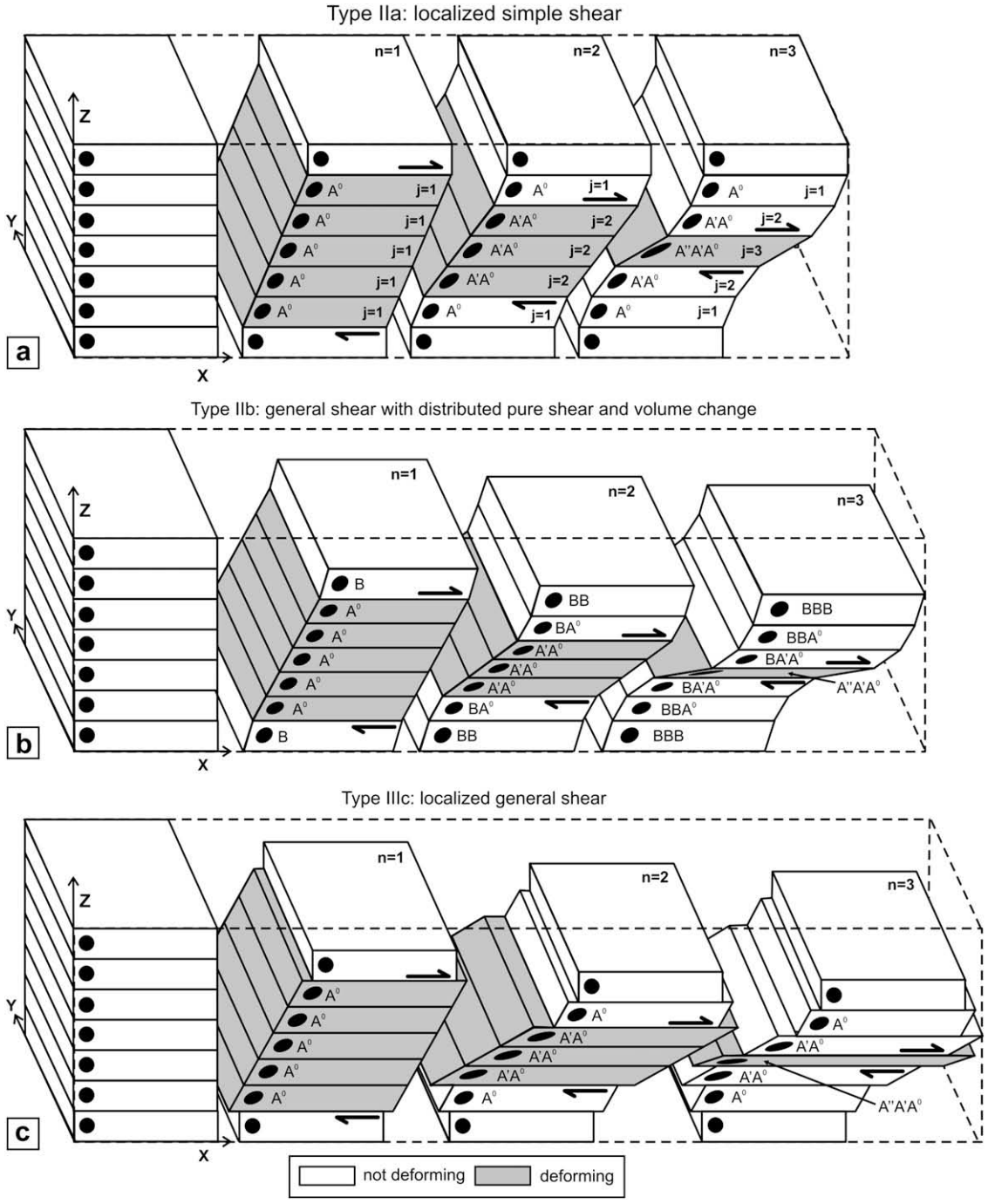

Fig. 3. Schematic evolution of shear zones characterized by decreasing thickness with time (shear strain softening). Each layer is labelled as the product of the incremental strain matrix (see text). (a) Type IIa: localized simple shear. (b) Type IIb: localized general shear with distributed pure shear and volume change. (c) Type IIc: localized general shear.

where the shear strain component (effective shear strain Γ) is a function of time t:

$$\Gamma_{\text{hard}}(t) = \frac{\gamma(t)(k_1 - k_3)}{\ln\left(\frac{k_1}{k_3}\right)} \text{ with } \gamma(t{+}1) < \gamma(t) \text{ for strain hardening models;}$$

$$\Gamma_{\text{soft}}(t) = \frac{\gamma(t)(k_1 - k_3)}{\ln\left(\frac{k_1}{k_3}\right)} \text{ with } \gamma(t{+}1) > \gamma(t) \text{ for strain softening models.}$$

The incremental strain matrix for bulk pure shear and volume change has the form:

$$B = \begin{pmatrix} k_1 & 0 & 0 \\ 0 & 1 & 0 \\ 0 & 0 & k_3 \end{pmatrix} \quad (6)$$

This matrix is not a function of time because strain hardening and softening have been postulated only for shear strain components.

After n steps the finite strain matrix representing the deformation of layer j for type Ib shear zones is:

$$A^*_{\mathrm{Ib}}(j) = \left(\prod_{i=0}^{n-j}\begin{pmatrix} k_1 & 1 & \Gamma_{\mathrm{hard}}(i) \\ 0 & 1 & 0 \\ 0 & 0 & k_3 \end{pmatrix}\right)\begin{pmatrix} k_1 & 0 & 0 \\ 0 & 1 & 0 \\ 0 & 0 & k_3 \end{pmatrix}^{j-1} = \left(\prod_{i=0}^{n-j} A(i)\right)B^{j-1} \quad (7)$$

with $1 \le j \le n$.

The geometric evolution is represented in Fig. 2(b), showing stretching along the shear direction and negative incremental volume change. In this model there is no strain incompatibility because pure shear and volume change components affect the whole rock volume.

In the case of pure shear alone (type Ib1) the finite strain matrix is:

$$A^*_{\mathrm{Ib1}}(j) = \left(\prod_{i=0}^{n-j}\begin{pmatrix} k_1 & 0 & \Gamma_{\mathrm{hard}}(i) \\ 0 & 1 & 0 \\ 0 & 0 & k_1^{-1} \end{pmatrix}\right)\begin{pmatrix} k_1 & 0 & 0 \\ 0 & 1 & 0 \\ 0 & 0 & k_1^{-1} \end{pmatrix}^{j-1} \quad (8)$$

whereas in the case of volume change alone (type Ib2) the finite strain matrix is:

$$A^*_{\mathrm{Ib2}}(j) = \left(\prod_{i=0}^{n-j}\begin{pmatrix} 1 & 0 & \Gamma_{\mathrm{hard}}(i) \\ 0 & 1 & 0 \\ 0 & 0 & 1+\Delta \end{pmatrix}\right)\begin{pmatrix} 1 & 0 & 0 \\ 0 & 1 & 0 \\ 0 & 0 & 1+\Delta \end{pmatrix}^{j-1} \quad (9)$$

For type IIb and IIb1 shear zones, taking into account the inverse order of deformed layers and the different effective shear strain function, the finite strain matrices are respectively:

$$A^*_{\mathrm{IIb}}(j) = \begin{pmatrix} k_1 & 0 & 0 \\ 0 & 1 & 0 \\ 0 & 0 & k_3 \end{pmatrix}^{j-1}\left(\prod_{i=0}^{n-j}\begin{pmatrix} k_1 & 0 & \Gamma_{\mathrm{soft}}(i) \\ 0 & 1 & 0 \\ 0 & 0 & k_3 \end{pmatrix}\right) = B^{j-1}\left(\prod_{i=0}^{n-j} A(i)\right) \quad (10)$$

and

$$A^*_{\mathrm{IIb1}}(j) = \begin{pmatrix} k_1 & 0 & 0 \\ 0 & 1 & 0 \\ 0 & 0 & k_1^{-1} \end{pmatrix}^{j-1}\left(\prod_{i=0}^{n-j}\begin{pmatrix} k_1 & 0 & \Gamma_{\mathrm{soft}}(i) \\ 0 & 1 & 0 \\ 0 & 0 & k_1^{-1} \end{pmatrix}\right) \quad (11)$$

whereas in the case of volume change alone (type IIb2 shear zones) the finite strain matrix is:

$$A^*_{\mathrm{IIb2}}(j) = \begin{pmatrix} 1 & 0 & 0 \\ 0 & 1 & 0 \\ 0 & 0 & 1+\Delta \end{pmatrix}^{j-1}\left(\prod_{i=0}^{n-j}\begin{pmatrix} 1 & 0 & \Gamma_{\mathrm{soft}}(i) \\ 0 & 1 & 0 \\ 0 & 0 & 1+\Delta \end{pmatrix}\right) \quad (12)$$

The geometric evolution is represented in Fig. 3(b) for $n = 3$.

2.3. Types Ic and IIc: localized general shear

For shear zones characterized by localized general shear, with no pure shear nor volume change components affecting the wall rock, the finite strain matrix is in the form of:

$$A^*_{\mathrm{Ic}}(j) = \prod_{i=0}^{n-j}\begin{pmatrix} k_1 & 0 & \Gamma_{\mathrm{hard}}(i) \\ 0 & 1 & 0 \\ 0 & 0 & k_3 \end{pmatrix} \quad (13)$$

for shear zones with increasing thickness (type Ic), and

$$A^*_{\mathrm{IIc}}(j) = \prod_{i=0}^{n-j}\begin{pmatrix} k_1 & 0 & \Gamma_{\mathrm{soft}}(i) \\ 0 & 1 & 0 \\ 0 & 0 & k_3 \end{pmatrix} \quad (14)$$

for shear zones with decreasing thickness (type IIc).

Figs. 2(c) and 3(c) show the geometric evolution of such shear zones, with stretching along the shear direction. In this case, strain incompatibility arises between adjacent layers because they are affected by different longitudinal strains and therefore they are characterized by different displacements. A similar incompatibility arises for localized general shear involving pure shear (types Ic1 and IIc1):

$$A^*_{\mathrm{Ic1}}(j) = \prod_{i=0}^{n-j}\begin{pmatrix} k_1 & 0 & \Gamma_{\mathrm{hard}}(i) \\ 0 & 1 & 0 \\ 0 & 0 & k_1^{-1} \end{pmatrix} \quad (15)$$

and

$$A^*_{\mathrm{IIc1}}(j) = \prod_{i=0}^{n-j}\begin{pmatrix} k_1 & 0 & \Gamma_{\mathrm{soft}}(i) \\ 0 & 1 & 0 \\ 0 & 0 & k_1^{-1} \end{pmatrix} \quad (16)$$

whereas there is no strain incompatibility in case localized general shear includes no longitudinal strain components but only the volume change (types Ic2 and IIc2):

$$A^*_{\mathrm{Ic2}}(j) = \prod_{i=0}^{n-j}\begin{pmatrix} 1 & 0 & \Gamma_{\mathrm{hard}}(i) \\ 0 & 1 & 0 \\ 0 & 0 & 1+\Delta \end{pmatrix} \quad (17)$$

and

$$A^*_{\mathrm{IIc2}}(j) = \prod_{i=0}^{n-j}\begin{pmatrix} 1 & 0 & \Gamma_{\mathrm{soft}}(i) \\ 0 & 1 & 0 \\ 0 & 0 & 1+\Delta \end{pmatrix} \quad (18)$$

2.4. Shear zone thickness and displacement

In order to define all the characteristics of type I (i.e. widening) shear zones, the following parameters must be taken into account: (i) original thickness (h) of each layer; (ii) number (n) of temporal steps; (iii) final shear zone displacement (D), and (iv) shear zone thickness (T). The latter two quantities may be written as a function of Γ and k_3. In order to provide a simple relationship between these quantities, we start from a finite strain matrix written as:

$$A^*(j) = \begin{pmatrix} k_1^* & 0 & \Gamma^*(j) \\ 0 & 1 & 0 \\ 0 & 0 & k_3^* \end{pmatrix} \quad (19)$$

and transform the original vector $\vec{F} = (0, 0, h)$ in the new vector:

$$\vec{F}^* = A^*(j)\cdot\vec{F} = \left(h\Gamma^*(j), 0, hk_3^*\right) \quad (20)$$

Then components of displacement of layer j parallel to the x axis is:

$$D_x(j) = h\Gamma^*(j) \quad (21)$$

The displacement components for a symmetric shear zone with an initial single layer ($j = 1$) are:

$$(D_x)_{SZ} = 2\sum_{j=1}^{n} h\Gamma^*(j) - h\Gamma^*(j = 1) \quad (22)$$

The thickness of each layer is:

$$T(j) = hk_3^* \quad (23)$$

whereas whole shear zone thickness is given by:

$$(T)_{\text{type 1}} = 2\sum_{j=1}^{n} hk_3^* - hk_3^* = (2n-1)hk_3^* \quad (24)$$

For type II models (i.e. thinning shear zones) it is necessary to distinguish: (i) the active shear zone, where deformation is occurring at a given time, and (ii) the whole shear zone, comprising the active portion as well as the inactive margins. The active shear zone thickness decreases with time, reaching the model limit value of hk_3^*:

$$(T)_{\text{active type II}} = (2(n-j)+1)hk_3^* \tag{25}$$

The displacement is that produced by the active shear zone:

$$(D_x)_{\text{active type II}} = \Gamma^*(j)(2(n-j)+1)hk_3^* \tag{26}$$

Whole shear zone thickness is given by Eq. (24), and the related displacement integrates all the contributions of the active shear zone through time:

$$(D_x)_{\text{whole type II}} = \sum_{j=1}^{n} \Gamma^*(j)(2(n-j)+1)hk_3^* \tag{27}$$

3. Heterogeneous shear zones involving shear strain hardening/softening

The function $\gamma(t)$ describing the temporal dependence of shear strain can be expressed in several forms. However, in order to take into account strain hardening/softening, it must be a decreasing/increasing monotonic function of time. A simple function of this type may be used to check the shear zone models considered in the previous sections. An exponential function is the simplest law simulating a constantly decreasing or increasing rate. Therefore, in this study we used a function in the form:

$$\gamma(t) = \gamma_0 e^{\alpha t} \tag{28}$$

where γ_0 is the initial shear strain increment and α is a constant defining the rate of strain hardening (for negative values) or softening (for positive values). In order to furnish realistic data, low incremental values of elongation and volume change have been considered ($k_1 = 1.01$ and $\Delta = -0.01$, the latter representing true volume change as there is no deformation along the y axis of the coordinate system).

To compare our theoretical models with natural shear zones, in Figs. 4–7 shear zone thickness (T) and displacement (D), expressed in meters, have been plotted in bilogarithmic diagrams and compared with similar plots derived by Hull (1988). The latter author showed how the best-fit regression of displacement/thickness data, coming from both brittle and ductile natural shear zones exposed in several orogens, is close to be linear over several orders of magnitude in size. Following Hull (1988), mylonitic (MSZ) and brittle (BSZ) shear zones are distinguished based on shear strain values. The former are characterized by γ ranging between 0.1 and 10 (low D/T ratio), whereas the latter shows γ in the range of 10–1000 (high D/T ratio).

To completely describe these models, several parameters were calculated: (i) the strain ratio R_{xz} of the finite strain ellipse in the principal XZ plane of the finite strain ellipsoid, (ii) the angle θ' (shear angle) that the finite strain ellipse long axis (X) forms with the shear direction (x axis of the coordinate system).

The finite strain matrix for all models is in the general form:

$$A^* = \begin{pmatrix} k_1^* & 0 & \Gamma^* \\ 0 & 1 & 0 \\ 0 & 0 & k_3^* \end{pmatrix} \tag{29}$$

The matrix eigenvalues correspond to the quadratic principal finite strain ellipsoid axes: γ_1^*, γ_2^* and γ_3^*. In this case, $\gamma_2^* = 1$ as there is no deformation along the y axis. Eigenvalues are calculated using the equation (Fossen and Tikoff, 1993):

$$\lambda_{1,3}^* = \frac{1}{2}\left(\Gamma^{*2} + k_1^{*2} + k_3^{*2} \pm \sqrt{-4k_1^{*2}k_3^{*2} + \left(\Gamma^{*2} + k_1^{*2} + k_3^{*2}\right)^2}\right) \tag{30}$$

with $\lambda_1^* > 1 > \lambda_3^*$. The finite strain ratio R_{XZ}^* is:

$$R_{XZ}^* = \sqrt{\frac{\lambda_1^*}{\lambda_3^*}} \tag{31}$$

The angle $\theta^{*\prime}$ is related to the previously defined parameters by the equation (Fossen and Tikoff, 1993):

$$\theta^{*\prime} = \arctan\left(-\frac{\Gamma^{*2} + k_1^{*2} - \lambda_1^*}{k_3^*\Gamma^*}\right) \tag{32}$$

3.1. Type Ia, Ib and Ic shear zones

For all models, an original layer thickness of 0.1 m and 10 time steps have been considered. Fig. 4 (a, b) shows a shear zone of type Ia (localized simple shear model) characterized by $\alpha = -1$ and γ_0 values of 0.1 and 10. Initial shear strain increments of 0.1 and 10 have been chosen so that the related curves start from the lower boundaries of the MSZ and BSZ fields (Hull, 1988), respectively. In both cases, the relationship between displacement and shear zone thickness is close to linear. The finite shear strain curve shows a classic flat-topped shape with a limit value of shear strain that holds constant with time. However, for a given number of steps (10 in this instance) and for a value of the parameter α characterizing the rate of strain hardening/softening as equal to -1, this configuration does not allow the system to reach large strains, as it is marked by short strain paths in the R_{xz}^*–θ' diagram. In order to provide a larger range of R_{xz}^* and Γ^* values, a value of the parameter $\alpha = -0.1$ has also been used (Fig. 4c, d). In this case, the finite shear strain and strain ratio curves are not flat-topped; rather, they show a general angular shape with a maximum in the middle, becoming flattened again when increasing the number of time steps. The thickness–displacement curve is not parallel to MSZ and BSZ field boundaries but remains inside the related fields. In order to obtain even larger strains it is necessary to increase the number of steps and to choose a value of the parameter α close to zero. For example, for 100 steps and $\alpha = -0.001$ (Fig. 4 e, f), the displacement/thickness curves plot over the entire range of shear strain values for mylonitic (MSZ) and brittle (BSZ) fields. For the latter configuration, the finite effective shear strain curves show straight limbs, whereas the finite ellipticity curves display a peaked shape with a rightward concavity.

Concerning type Ib shear zones, in order to simplify the analysis, only sub-types Ib1 and Ib2 have been considered. The diagrams of Fig. 5 show the results of the analysis for the mylonitic field (MSZ) only, curve shapes being similar for the brittle (BSZ) field (although with different absolute values). For a type Ib1 shear zone (localized general shear and diffuse pure shear model) with $\gamma_0 = 0.1$, $\alpha = -1$, $k_1 = 1.01$ and $\Delta = 0$, the relationship between displacement and shear zone thickness is about linear and the curve lies within the MSZ field (Fig. 5a). Finite effective shear strain and ellipticity curves display an angular shape with straight limbs. As in the previous model, short strain paths result in the R_{xz}^*–θ' diagram. For a similar model but with $\alpha = -0.1$, the finite effective shear strain curve is angular with rounded limbs, whereas the finite strain ratio curve

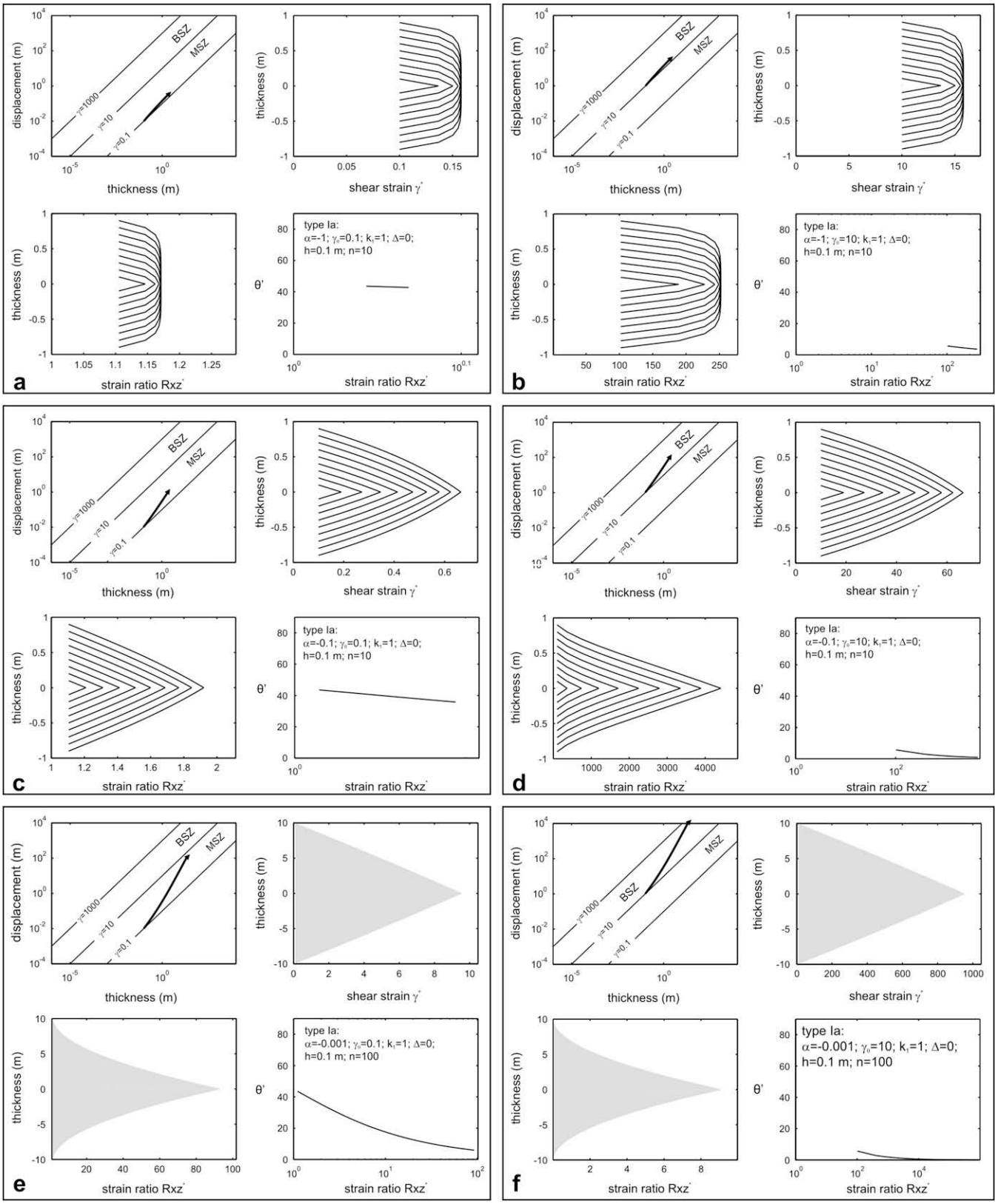

Fig. 4. Type Ia shear zones: diagrams of shear zone thickness *versus* displacement (boundaries of MSZ and BSZ fields are from Hull, 1988), finite shear strain and strain ratio *versus* thickness; and diagrams of finite strain ratio *versus* angle θ'. (a) Mylonitic shear zone with strong strain hardening. (b) Brittle shear zone with strong strain hardening. (c) Mylonitic shear zone with weak strain hardening. (d) Brittle shear zone with weak strain hardening. (e) Mylonitic shear zone with very weak shear strain hardening. (f) Brittle shear zone with very weak shear strain hardening.

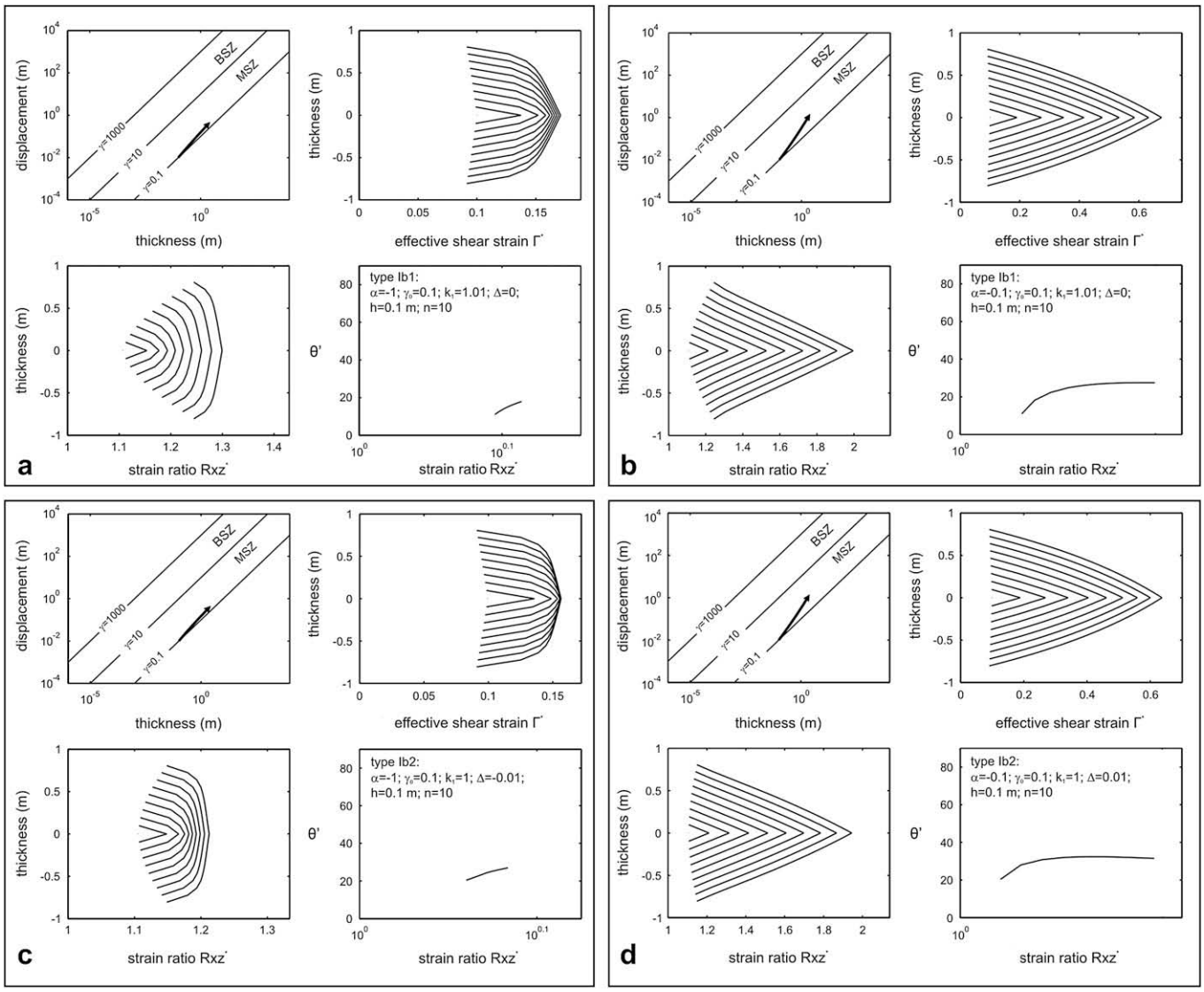

Fig. 5. Type Ib shear zones: diagrams of shear zone thickness *versus* displacement, finite effective shear strain and strain ratio *versus* thickness; and diagrams of finite strain ratio *versus* angle θ'. (a) Type Ib1 mylonitic shear zones with strong strain hardening. (b) Type Ib1 mylonitic shear zones with weak strain hardening. (c) Type Ib2 mylonitic shear zones with strong strain hardening. (d) Type Ib2 mylonitic shear zones with weak strain hardening.

displays essentially straight limbs (Fig. 5b). The strain paths in the R^{*}_{xz}–θ' diagram encompass larger values of finite strain ratio with respect to the previous model.

For a type Ib2 shear zone (localized general shear and diffuse volume change model) with $\alpha = -1$, $\Delta = -0.01$ and $k_1 = 1$, the plots are similar to the former configuration (Fig. 5c). For $\alpha = -0.1$, as in previous models, the curves show a general angular shape (Fig. 5d).

For type Ic shear zones, in order to simplify the analysis, only sub-types Ic1 and Ic2 have been considered. The results are shown for the mylonitic field (MSZ) field in the diagrams of Fig. 6. For type Ic1 shear zones (synchronous localized simple and pure shear model) with $\gamma_0 = 0.1$, $\alpha = -1$, $k_1 = 1.01$ and $\Delta = 0$, the relationship between displacement and shear zone thickness (Fig. 6a) is similar to the previous configuration (type Ib2 shear zones). The finite effective shear strain and strain ratio curves show an angular shape with straight limbs in the central sector, and a curved shape close to the margins. With $\alpha = -0.1$ the finite effective shear strain and strain ratio curves show an angular shape, with slightly rounded limbs (Fig. 6b). For both models the finite elongation is not constant across the shear zone; rather, it increases from the margins to the centre, and each layer is characterized by a different displacement that must be accommodated by discontinuities (*cream cake effect*). For a shear zone of type Ic2 (synchronous localized simple shear and volume change model), with $\alpha = -1$, $\Delta = -0.01$ and $k_1 = 1$, the curve of finite strain ratio is similar to the former configuration; however, the finite effective shear strain curve shows a flat-topped shape (Fig. 6c). With $\alpha = -0.1$ the finite strain ratio and effective shear strain curves display again an angular shape (Fig. 6d). The curve of finite volume change across the shear zone shows a linear decrease toward the middle of the shear zone for each time step. However, in this instance strain compatibility is maintained since there is no elongation along the shear direction.

3.2. Type IIa, IIb and IIc shear zones

For type II shear zones, in order to have a displacement–shear zone thickness curves falling into the MSZ and BSZ fields, a maximum value of the parameter α equal to 0.4 has been adopted. Further parameters are the same as for previous models. In all models (types IIa, IIb1, IIb2 and IIc shear zones), the displacement–thickness relationship for the active shear zone is first negative (the thickness increasing as the displacement decreases) and then

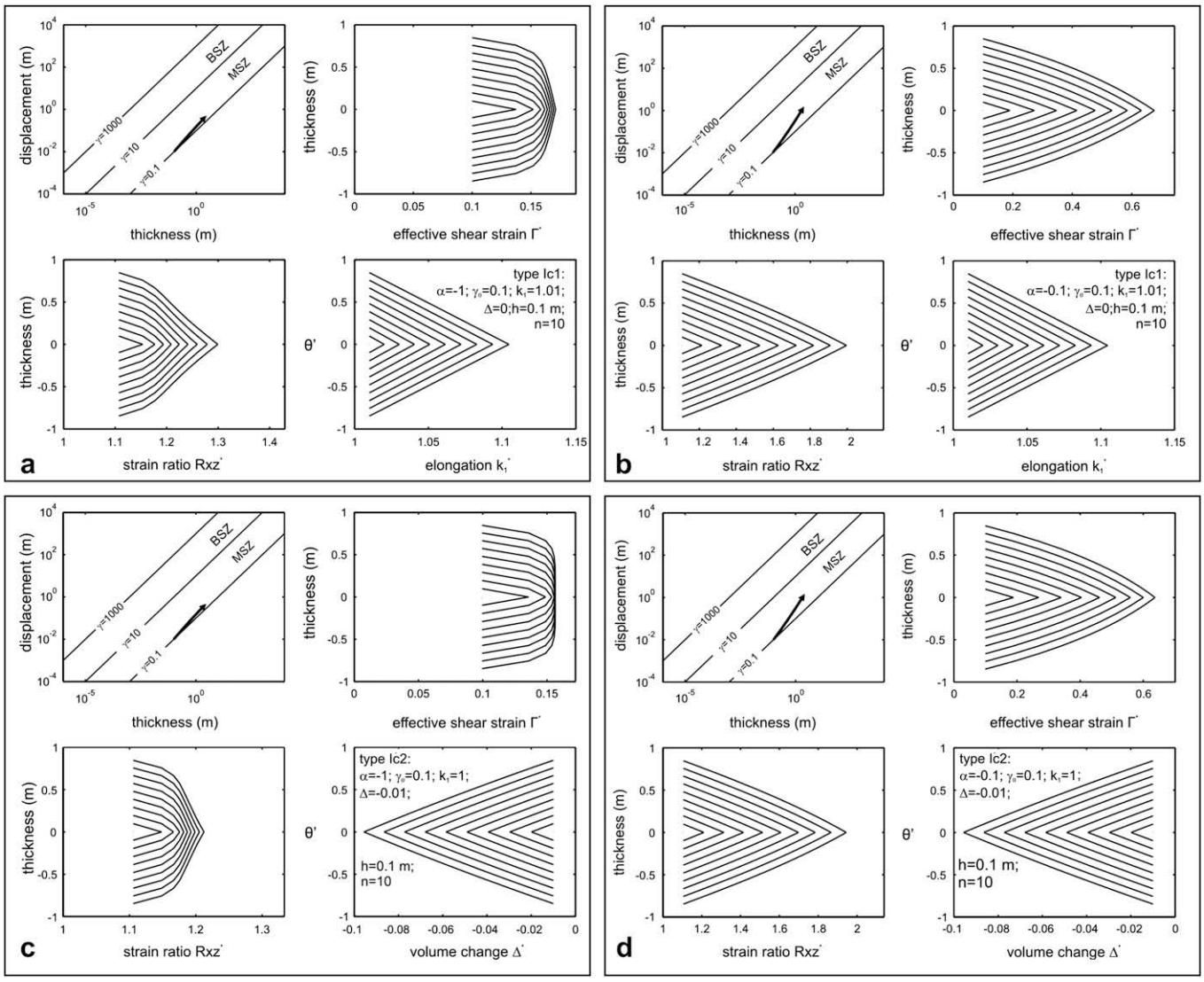

Fig. 6. Type Ic shear zones: diagrams of shear zone thickness *versus* displacement; and diagrams of finite effective shear strain, strain ratio, elongation/volume change *versus* thickness. (a) Type Ic1 mylonitic shear zones with strong strain hardening. (b) Type Ic1 mylonitic shear zones with weak strain hardening. (c) Type Ic2 mylonitic shear zones with strong strain hardening. (d) Type Ic2 mylonitic shear zones with weak strain hardening.

positive as both thickness and displacement decrease (Fig. 7). On the other hand, the whole shear zone thickness holds constant (type IIa; Fig. 7a, b) or weakly decreases in case pure shear components are involved (types IIb, IIc; Fig. 7c–f). Finite shear strain, effective shear strain and strain ratio curves show a narrow peaked shape with a rightward concavity, covering the whole MSZ range of γ values for all models. Lower amounts of strain would be obtained, for the same time steps, in case value of $\alpha < 0.4$ is used.

3.3. Shear zone thickness–displacement relationships

In order to investigate the relationships between shear zone thickness and displacement, *T–D* diagrams have been constructed for values of γ_0 of 0.1 and 10, with varying initial layer thickness (h values of 0.01, 0.1, 1 and 10 m). As an example, in Fig. 8 (a) the behaviour of type Ia shear zones is shown. The other investigated shear zone types yield similar curves.

3.4. Displacement and shear strain rates

The parameter α of the exponential law controlling shear strain hardening/softening influences the temporal variation of all strain parameters. For each layer included in the shear zone, geometric and kinematic characteristics of the deformation change with time due to the non-constant value of the incremental shear strain. Therefore, deformation is not steady state. To analyze the role of the parameter α on kinematic quantities such as displacement and shear strain rates, the first derivative with respect to time (steps) has been calculated for the mean shear strain (Γ_m) obtained as the ratio between displacement and final shear zone thickness. As an example this has been carried out for initial shear strain increment values of 0.1 (mylonitic shear zone models), using $\alpha = -0.1$ (strain hardening) and $\alpha = 0.4$ (strain softening) for types Ia and IIa shear zones, respectively. Note that the curves in Fig. 8 (b) are independent of the original shear zone thickness (h).

4. Discussion

Our models describe non-homogeneous shear zones whose thickness changes with time. Modelled shear zones consist of a series of homogeneously deformed layers characterized by no deformation along the y axis. The pure shear component of the deformation, when present, is accommodated by stretching along the shear direction, whereas strain hardening/softening regards

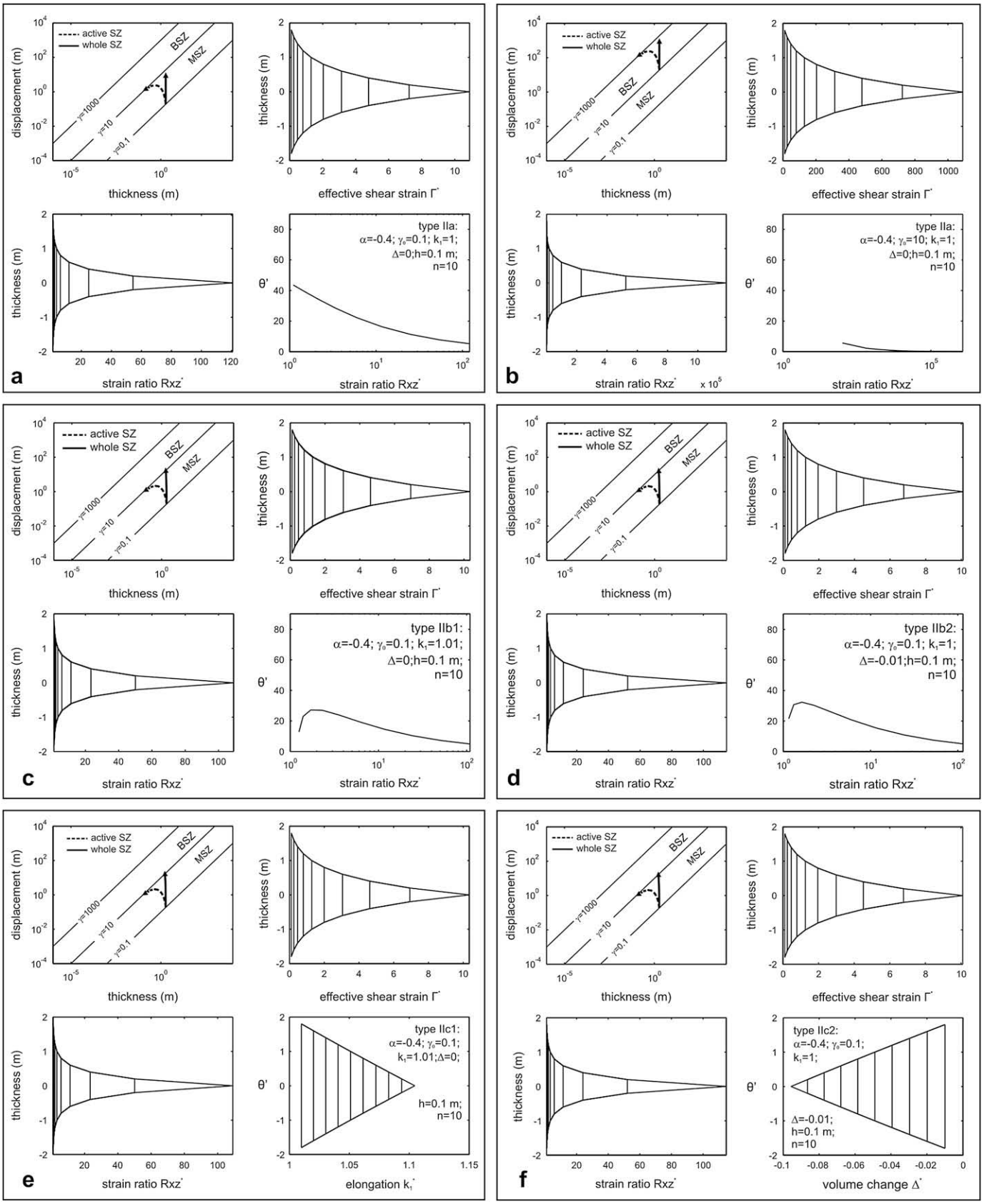

Fig. 7. Type II shear zones: diagrams of shear zone thickness *versus* displacement; diagrams of finite shear strain/effective shear strain, strain ratio, elongation/volume change *versus* thickness; and diagrams of finite strain ratio *versus* angle θ'. (a) Type IIa mylonitic shear zones. (b) Type IIa brittle shear zones. (c) Type IIb1 mylonitic shear zones. (d) Type IIb2 mylonitic shear zones. (e) Type IIc1 mylonitic shear zones. (f) Type IIc2 mylonitic shear zones.

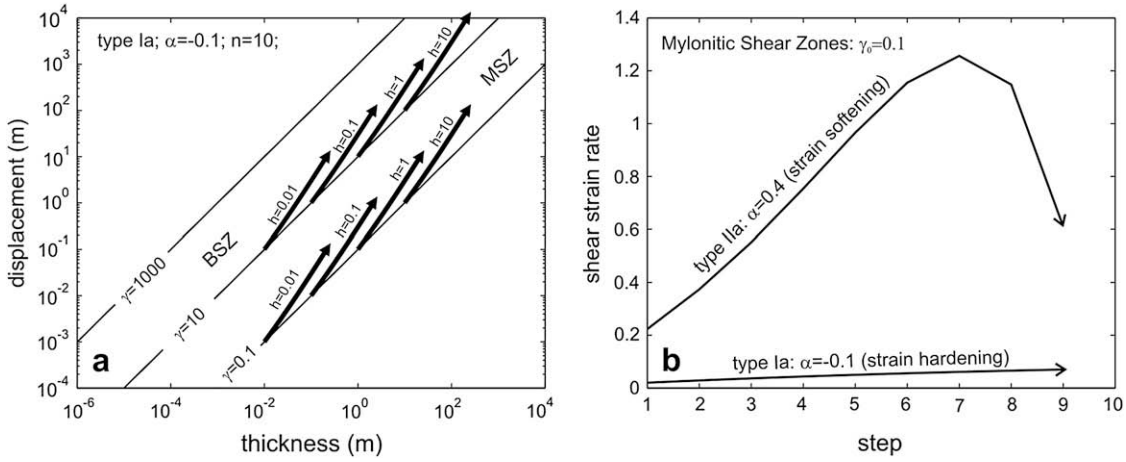

Fig. 8. (a) Diagram of shear zone thickness *versus* displacement for type Ia mylonitic (MSZ) and brittle (BSZ) shear zones, with initial layer thickness of 0.01, 0.1, 1 and 10 m. (b) Diagrams of time steps *versus* shear strain rate for type Ia shear zones (with weak strain hardening) and for type IIa shear zones.

uniquely the shear strain component. Each layer is characterized by a finite deformation expressed as a finite product of incremental strain matrices. By modelling strain hardening/softening using an exponential function, it has been possible to provide theoretical profiles of finite effective shear strain and finite strain ratio across different shear zone types. The function exponent α is related to the rate of shear strain hardening (negative values) or softening (positive values), and influences all further strain parameters. For instance, a value of $\alpha = -0.1$ (weak shear strain hardening) implies that the simple shear component prevails over the pure shear and volume change components. Conversely, a lower value (such as $\alpha = -1$) disallows the simple shear component (strong shear strain hardening). For the strain softening case, a maximum value of $\alpha = 0.4$ has been used to allow displacement/thickness curves to fall into the mylonitic (MSZ) and brittle (BSZ) shear zone fields as defined by Hull (1988).

The relationship existing between shear zone displacement and thickness depends both on the parameter α and on the initial shear strain increment γ_0 imposed to each layer at time $t = 0$. This relationship is always positive for widening shear zones (type I, $\alpha < 0$), with the parameter α controlling the slope of the curves. For thinning shear zones (type II, $\alpha > 0$), the displacement–thickness relationship is first negative and subsequently positive for the actively deforming shear zone. On the other hand, the displacement–thickness curve for the whole shear zone is either parallel to the ordinate axis (i.e. constant thickness) or with a negative steep slope.

The other significant parameter is the initial shear strain increment controlling whether a shear zone plots within the ductile (MSZ) or brittle (BSZ) fields (Figs. 4–8). In particular, all shear zones plot within the MSZ field for a chosen initial shear strain increment value of 0.1, whereas they plot into the BSZ field for an initial shear strain increment value of 10, independently of the original thickness (h) of the shear zone (Fig. 8a).

Types Ia and IIa shear zones represent the 'classical' shear zones in which deformation is accommodated by heterogeneous simple shear. For the type Ia increasing thickness is driven by shear strain hardening, whereas for type IIa decreasing thickness is due to shear strain softening. The flat-topped shape of the finite shear strain curve across type I shear zones characterized by strong strain hardening (Fig. 4a, b) shows how shear zone evolution involves a progressive deactivation of the strain-hardened inner sector, while deformation propagates into the shear zone margins. The evolution with time of the shear strain profile, shows a transition from an original peaked shape to a flat-topped shape, conforms to that classically described for type I shear zones (Fig. 1). For type Ia shear zones (weak strain hardening), the shear strain curve displays an angular shape (Fig. 4c, d). This feature indicates that deformation takes place in the inner part of the shear zone for a long time, the shear strain and strain ratio curves becoming flattened only after a large number of time steps. For type IIa shear zones, shear strain and strain ratio profiles consistently show a characteristic, narrow peaked shape, with a large range of ellipticity values (Fig. 7a, b).

Types Ib and IIb shear zones are characterized by localized general shear and distributed pure shear and/or volume change. For a small component of either incremental elongation or volume change, and for a strong strain hardening, the profiles of effective shear strain and strain ratio tend to attain an angular shape with straight limbs (Fig. 5a, c). This means that, after a given time, a balance between simple shear and pure shear/volume change components is reached, holding to a constant increase of effective shear strain from the margins to the inner sector of the shear zone. For weak shear strain hardening, the effective shear strain and strain ratio curves display more rounded shapes; however, after a large number of time steps, also these profiles tend to attain straight limbs (Fig. 5b, d). As in the previous model, for type IIb shear zones effective shear strain and ellipticity profiles display an angular shape, suggesting that the presence of pure shear and/or volume change components does not significantly influence the overall characteristics of finite strain parameters.

Type Ic and IIc shear zones are characterized by localized general shear involving simultaneous: (i) simple shear and pure shear (types Ic1 and IIc1), (ii) simple shear and volume change (types Ic2 and IIc2), or (iii) simple shear, pure shear and volume change. In case (i) and for strong strain hardening after a given time the effective shear strain and strain ratio curves display an angular shape with straight limbs (Fig. 6a), as in the previous model. However, in this case there is strain incompatibility between the layers. For weak shear strain hardening the profiles of effective shear strain and strain ratio are rounded (Fig. 6b). In case (ii) and for strong strain hardening the effective shear strain curve shows again a flat-topped shape, whereas the strain ratio profile displays straight limbs after a given time (Fig. 6c) and strain compatibility is maintained between the layers. For weak shear strain the profiles of effective shear strain and strain ratio are rounded (Fig. 6d). For type IIc shear zones, the presence of localized pure shear and/or volume change components again does not vary the general shape of

effective shear strain and ellipticity curves, although incompatibility between layers, characterized by different finite strain, arises.

Taking into account all possible configurations for the strain hardening models, it is worth noting that the classic flat-topped shape of the effective shear strain curve, characteristic of type I shear zones as reported in previous papers, is actually distinctive of types Ia and Ic2 only. More frequently, a peaked shape is obtained, whereas for type II shear zones the shear strain and especially the ellipticity profiles display always a narrow angular shape with concavity toward the right. Shear strain rates (Fig. 8b) always increase with time for type Ia shear zones, tending asymptotically to a constant value for a large number of time steps. Conversely, for type IIa shear zones the curve shows a well-defined maximum and is characterized by higher values with respect to the previous model.

In order to compare our modelling results with natural shear zones, some considerations about the possible real values of the time unit (step) introduced in the models are noteworthy. For example, shear strain rates for structures plotting within the MSZ field and characterized by weak shear strain hardening ($\alpha = -0.1$) show a mean value of 0.04 step^{-1}, whereas for shear strain softening ($\alpha = 0.4$) a mean value of 0.70 step^{-1} (Fig. 8b). By comparing these values with a shear strain of 10^{-13} s^{-1} (i.e. within the range of typical values of natural ductile shear zones; Schmid, 1975; Pfiffner and Ramsay, 1982; Hacker et al., 1992; Vitale et al., 2007), the time step of our models may be estimated as of *ca*. 10^4–10^5 years. Related maximum displacement rates attain values of 0.01 and 0.10 mm/year for mylonitic widening and thinning shear zones, respectively. For brittle structures, maximum displacement rates are of 1 mm/y for widening shear zones, and 10 mm/y for thinning ones.

A few interesting considerations may arise by comparing strain hardening and softening models, as discussed in the following points.

(1) The geometric finite configurations are essentially similar for both models, being the same for types Ia and IIa (Figs. 2, 3). In order to distinguish the driving mechanism (strain hardening or softening), the shear strain profile across the shear zone needs to be analyzed. However, the profiles obtained in case pure shear and volume change components, and/or variable amounts of strain hardening are involved in the deformation, show more complex patterns with respect to the curves described by Hull (1988). In particular, as peaked-shaped curves are not restricted to the strain softening case, the simple criterion of flat-topped *versus* peaked-shaped curves is not sufficient to distinguish between widening and thinning shear zones.

(2) Both strain hardening and softening models fit the data obtained from natural shear zones, *T*–*D* curves falling into the mylonitic and brittle fields defined by Hull (1988). However, in order to encompass the whole range of natural shear strains (from $\gamma = 0.1$ to $\gamma = 10$ for mylonitic shear zones, and from $\gamma = 10$ to $\gamma = 1000$ for brittle ones), strain hardening models must be working for a long time. The example of Fig. 4 (e, f) shows that, even for a very weak strain hardening ($\alpha = -0.001$), a large number of steps ($n = 100$, i.e. 10^6–10^7 years) are needed to obtain curves extending over the entire MSZ and BSZ fields. On the other hand, strain softening models require a time span of one order of magnitude less to achieve comparable finite strains.

(3) Both models allow for a maximum variation of three orders of magnitude in size of both thickness and displacement (Figs. 4–8). Therefore, based on our results, the question posed by Hull (1988) of whether large shear zones can grow from smaller ones might be affirmatively answered, although it is envisaged that the process could occur only within a limited size range.

5. Conclusions

Mathematical models may be effectively used to describe the theoretical behaviour of heterogeneous shear zones characterized by increasing (type I) or decreasing (type II) thickness with time. Shear zone modelling may be carried out by taking into account different types and degrees of localization of the deformation, assuming decreasing or increasing shear strain rate due, to shear strain hardening or softening, respectively. In these conditions, the shear strain must be a monotonic function of time. In this study, a simple exponential function is used to allow for comparison with real quantities for different shear zone types. With respect to previous models of type I shear zones, classically characterized by a flat-topped shear strain profile across the shear zone (Hull, 1988), our study indicates that they may also display a peaked-shaped curve in case pure shear and/or volume change components are present. Conversely, type II shear zones are consistently characterized by angular shaped profiles with a rightward concavity.

All models depend on a series of parameters such as: (i) the exponent of the shear strain-time function, (ii) the initial shear strain increment imposed to the system, and (iii) the thickness of each homogeneously deformed layer composing the shear zone. By varying these parameters it is possible to model weak or strong shear strain hardening/softening, as well as the relationship between displacement (D) and shear zone thickness (T). This allows for a quantitative description of brittle and ductile shear zone behaviours, these being characterized by high and low D/T ratio, respectively.

Comparing mean shear strain rates for type Ia and IIa shear zones with a mean value of 10^{-13} s^{-1} (compatible with natural ductile shear zones), our models yield maximum displacement rates of 0.01 (for widening shear zones) and 0.10 (for thinning shear zones) mm/y for mylonitic structures, and of 1 (for widening shear zones) and 10 (for thinning shear zones) mm/y for brittle features, both regardless of shear zone thickness. Our results confirm that theoretical modelling of heterogeneous shear zone behaviour may provide useful insights into the modes of finite strain and displacement accumulation in ductile and brittle shear zones.

Acknowledgements

We thank V. Guerriero for helpful discussions and JSG reviewers J.-L. Bouchez, T. Takeshita, and associate editor J. Hippertt, for the useful comments that allowed us to significantly improve the paper.

References

Baird, G.B., Hudleston, P.J., 2007. Modeling the influence of tectonic extrusion and volume loss on the geometry, displacement, vorticity, and strain compatibility of ductile shear zones. Journal of Structural Geology 29, 1665–1678.

Fossen, H., Tikoff, B., 1993. The deformation matrix for simultaneous simple shearing, pure shearing and volume change, and its application to transpression–transtension tectonics. Journal of Structural Geology 15, 413–422.

Hacker, B.R., Yin, A., Christie, J.M., Davis, G.A., 1992. Rheology of an extended middle crust inferred from quartz grain sizes in the Whipple Mountains, California. Tectonics 11, 36–46.

Horsman, E., Tikoff, B., 2007. Constraints on deformation path from finite strain gradients. Journal of Structural Geology 29, 256–272.

Hull, J., 1988. Thickness–displacement relationships for deformation zones. Journal of Structural Geology 10, 431–435.

Means, W.D., 1984. Shear zones of types I and II and their significance for reconstruction of rock history. Geological Society of America Abstracts 16, 50.

Means, W.D., 1995. Shear zones and rock history. Tectonophysics 247, 157–160.

Pfiffner, O.A., Ramsay, J.G., 1982. Constraints on geological strain rates: arguments from finite strain states of naturally deformed rocks. Journal of Geophysical Research 87, 311–321.

Ramsay, J.G., 1980. Shear zone geometry: a review; shear zones in rocks. Journal of Structural Geology 2, 83–99.

Ramsay, J.G., Graham, R.H., 1970. Strain variation in shear belts. Canadian Journal of Earth Sciences 7, 786–813.

Ramsay, J.G., Huber, M., 1987. Folds and Fractures. In: The Techniques of Modern Structural Geology, vol. I. Academic Press, London.
Ring, U., 1998. Volume strain, strain type and flow path in a narrow shear zone. Geol Rundsch 86, 786–801.
Schmid, S., 1975. The Glarus overthrust: field evidence and mechanical model. Eclogae Geologicae Helvetiae 68, 247–280.
Srivastava, H.B., Hudleston, P., Earley III, D., 1995. Strain and possible volume loss in a high-grade ductile shear zone. Journal of Structural Geology 17, 1217–1231.
Vitale, S., White, J.C., Iannace, A., Mazzoli, S., 2007. Ductile strain partitioning in micritic limestones, Calabria, Italy: the roles and mechanisms of intracrystalline and intercrystalline deformation. Canadian Journal of Earth Sciences 44, 1587–1602.